International Journal of Environmental Sciences
ISSN: 2229-7359
Vol. 11 No. 22s, 2025
https://theaspd.com/index.php

Development and Optimization of Herbal Hydrogel for Wound Healing Activity

Mr. Amol V. Supekar[1], Dr. Sanjay Bhawar[2]
[1]Research Scholar, Bhagwant University, Ajmer, India
[2]Professor and Principal, Pravara Rural College of Pharmacy, Loni, Maharashtra, India
Corresponding author
Mr. Amol V. Supekar[1]
Email ID: supekaramol123@gmail.com
Address: Research Scholar, Bhagwant University, Ajmer, India

Abstract
Objectives: *The present study aimed to formulate and optimize a herbal hydrogel loaded with Azadirachta indica leaf extract (AILE), Moringa oleifera fruit shell extract (MFSE), and Ruellia prostrata leaf extract (RPLE) for enhanced anti-inflammatory and wound healing activity, utilizing natural bioactives in a topical delivery system.* ***Methods:*** *Hydrogels were prepared using Carbopol 940 and Carveol as the gelling agent and penetration enhancer, respectively. A 3^2 factorial design was employed to evaluate the effect of polymer and enhancer concentrations on key responses including viscosity and drug release at 12 hours. Preformulation studies including solubility (Table 3), FTIR (Figure 2), and DSC (Figure 1) were performed. The optimized batch was selected based on desirability function and validated experimentally (Table 9). The formulation was further evaluated for physicochemical parameters (Tables 4–5), ex vivo permeation (Table 5a), kinetic modeling (Table 6), anti-inflammatory (Tables 10–12), wound healing (Table 13), and stability (Table 14) studies.* ***Results:*** *The optimized batch F6 showed viscosity of 7786 cP and 76.35% drug release at 12 hours with a low prediction error (4.0% and 0.72%, respectively). Ex vivo studies revealed high flux (57.82 µg/cm²/h) and permeability coefficient (5.78×10^{-3} cm/h). In vivo studies demonstrated 15.87% and 14.32% inhibition of edema in carrageenan and CFA models, respectively. F3 formulation exhibited synergistic anti-inflammatory effect (75.83%) and significant cell viability (153%) in wound healing assay. The formulation remained stable for 3 months under both storage conditions.* ***Conclusion:*** *The optimized hydrogel formulation exhibited promising anti-inflammatory and wound healing efficacy, supported by permeation and biological data, suggesting strong potential for future clinical translation as a topical herbal therapy.*
Keywords:*Herbal hydrogel, factorial design, anti-inflammatory, wound healing, AILE, MFSE, RPLE, optimization, permeation.*

INTRODUCTION

Wound healing is a complex biological process essential for restoring skin integrity after injury, yet it remains a significant global health concern, particularly in developing nations where chronic wounds, diabetic ulcers, and infections are prevalent [1]. The World Health Organization estimates that chronic wounds affect over 100 million people worldwide annually, contributing substantially to healthcare expenditures and morbidity [2]. In the United States alone, wound management costs exceed $25 billion each year, with similar economic burdens reflected globally [3]. Conventional wound healing treatments, including antibiotics and corticosteroids, often pose limitations such as drug resistance, delayed healing, and local irritation. Furthermore, current synthetic formulations may lack bioactivity or fail to adequately support tissue regeneration [4]. Emerging infections and antibiotic resistance further exacerbate the therapeutic challenge. Recent trends have shifted focus toward plant-based therapeutics due to their safety profile, cost-effectiveness, and multi-targeted healing mechanisms [5]. However, the translation of herbal efficacy into stable, effective topical delivery systems remains inadequately explored, underscoring the urgent need for innovative and synergistic wound care solutions [6].

Azadirachta indica (Neem), Myristica fragrans (Nutmeg), and Ruellia prostrata are ethnomedicinally acclaimed plants with well-documented wound healing properties. Azadirachta indica is rich in nimbidin, quercetin, and flavonoids, known for their antimicrobial, anti-inflammatory, and antioxidant activities [7]. Myristica fragrans contains myristicin, elemicin, and eugenol, which inhibit pro-inflammatory mediators and promote tissue regeneration. Ruellia prostrata is reported to contain flavonoids, triterpenoids, and phenolic acids that contribute to fibroblast proliferation and angiogenesis. Collectively, these phytoconstituents exhibit strong potential in modulating multiple phases of the wound healing

cascade [8]. Prior in vitro and in vivo studies have validated the individual bioactivities of these plant extracts; however, their combined, synergistic action in a topical hydrogel system remains underexplored. The polyherbal synergy may amplify biological effects through complementary pathways such as free radical scavenging, cytokine inhibition, and enhanced cellular repair [9]. Therefore, integrating these plant extracts in a single formulation may offer a broad-spectrum, multi-functional, and biocompatible solution to accelerate wound healing and reduce infection-related complications [10]. Topical hydrogels have emerged as promising drug delivery systems in wound care due to their biocompatibility, hydration capability, ease of application, and sustained drug release properties. In this study, a polyherbal hydrogel was formulated using Carbopol 940 as a gelling agent and Carveol as a penetration enhancer [11]. The hydrogel matrix facilitates controlled release and optimal skin adherence while maintaining a moist wound environment, which is critical for tissue regeneration. Carbopol 940 contributes to suitable rheological behavior and stability, while Carveol enhances transdermal absorption by disrupting the lipid structure of the stratum corneum. Compared to conventional creams and ointments, the hydrogel offers enhanced bioavailability, targeted delivery, and minimal greasiness [12]. Recent advances in hydrogel technology emphasize the incorporation of multiple phytoconstituents into a stable and synergistic platform. This delivery approach ensures uniform dispersion of active agents, preserves their bioactivity, and extends contact time with the wound bed, making it ideal for polyherbal formulations aimed at comprehensive wound healing management [13].

The present study aims to develop, optimize, and evaluate a novel polyherbal hydrogel comprising Azadirachta indica, Myristica fragrans, and Ruellia prostrata for enhanced wound healing. Specific objectives include factorial-based formulation design, physicochemical characterization, ex vivo permeation analysis, and biological evaluation through in vivo anti-inflammatory and in vitro wound healing assays. This study explores phytosynergistic potential in a modern delivery matrix.

MATERIALS AND METHODS

MATERIALS

Azadirachta indica leaf extract (AILE), Moringa oleifera fruit shell extract (MFSE), and Ruellia prostrata leaf extract (RPLE), each standardized and authenticated, were obtained from Sciquaint Innovations (Pune, India). Carbopol 940 (analytical grade, viscosity 40,000–60,000 cP) and Carveol (analytical grade, ≥98% purity) were purchased from Sigma-Aldrich (St. Louis, USA). Triethanolamine (analytical grade, ≥99% purity, MW: 149.19 g/mol) and Propylene glycol (analytical grade, ≥99.5% purity, MW: 76.09 g/mol) were sourced from Loba Chemie Pvt. Ltd. (Mumbai, India). Ethanol and methanol (HPLC grade, purity ≥99.9%) were procured from Merck Life Science Pvt. Ltd. (Mumbai, India). Phosphate buffer components including monobasic potassium phosphate and sodium hydroxide (analytical grade) were obtained from S.D. Fine-Chem Ltd. (Mumbai, India). Carrageenan (Type I, analytical grade, molecular weight ~200,000–800,000) was purchased from HiMedia Laboratories Pvt. Ltd. (Mumbai, India). All other solvents and chemicals used in the study were of analytical grade and used without further purification. Double-distilled water was used throughout the experiments.

METHODS

Solubility study

The solubility of AILE, MFSE, and RPLE was evaluated in various solvents including distilled water, phosphate buffer (pH 6.8 and 7.4), acetate buffer (pH 4.5), methanol, ethanol, and propylene glycol. An excess amount of each extract was added to 5 mL of solvent in screw-capped vials and vortexed for 2 min, followed by shaking at 100 rpm in an orbital shaker (CIS-24BL, Remi, India) at 25 ± 1 °C for 24 h. After equilibrium, samples were centrifuged at 5000 rpm for 15 min and filtered through a 0.45 µm membrane filter. The filtrates were diluted appropriately and analyzed using a UV-Visible spectrophotometer (UV-1800, Shimadzu, Japan) at their respective λmax values. All measurements were performed in triplicate (n=3), and solubility was expressed as mg/mL [14,15].

Differential scanning colorimetry (DSC)

DSC was performed to evaluate the thermal compatibility between plant extracts and excipients using a differential scanning calorimeter (DSC 4000, Perkin Elmer, India). Samples (5–10 mg) of pure extracts, individual excipients, and their physical mixtures were accurately weighed and sealed in aluminum pans. The analysis was carried out from 25 °C to 300 °C at a heating rate of 10 °C/min under a nitrogen flow

of 20 mL/min. Thermograms were analyzed using Pyris software (v11.0) to observe any shifts in melting endotherms or new transitions. Each sample was tested in triplicate (n=3) to confirm consistency [16,17].

Fourier Transform Infrared (FTIR) Spectroscopy

FTIR analysis was carried out to identify functional groups and assess possible interactions between extracts and excipients. Spectra were recorded using an FTIR spectrophotometer (Alpha II, Bruker, India) equipped with an attenuated total reflectance (ATR) accessory. Samples of pure extracts, individual excipients, and their physical mixtures were placed directly on the ATR crystal and scanned over a wavenumber range of 4000–400 cm^{-1} with a resolution of 4 cm^{-1} and 16 scans per sample. All spectra were processed using OPUS software (v7.5). Each analysis was performed in triplicate (n=3) to ensure reproducibility and confirm peak consistency [18,19].

Experimental Design for Formulations

A 3^2 full factorial design was employed to optimize the hydrogel formulation. Two independent variables were selected: X_1 (carbopol 940 concentration) and X_2 (carveol concentration), each at three levels (low, medium, high). The dependent variables were Y_1 (viscosity) and Y_2 (drug release at 12 h). The mathematical relationship between the independent and dependent variables was established using the following polynomial equation:

$$Y = b_0 + b_1X_1 + b_2X_2 + b_{12}X_1X_2 + b_{11}X_1^2 + b_{22}X_2^2$$

Where Y is the dependent variable, b_0 is the intercept, b_1 and b_2 are the linear coefficients, b_{12} is the interaction coefficient, and b_{11} and b_{22} are the quadratic coefficients [20-22].

Table 1: Independent and Dependent Variables in 3^2 Factorial Design

Independent Variables	**Low (-1)**	**Medium (0)**	**High (+1)**
X_1: Carbopol 940 (% w/w)	0.5	1.0	1.5
X_2: Carveol (% w/w)	2	4	6
Dependent Variables			**Goal**
Y_1: Viscosity (cP)			Optimize
Y_2: Drug Release at 12 h (%)			Maximize

Preparation of Hydrogel Formulations

Hydrogels were prepared by the cold dispersion method as per the composition outlined in Table 2. Carbopol 940 was dispersed in 70 mL of distilled water and allowed to hydrate for 24 h at room temperature. Separately, AILE (1% w/w), MFSE (0.5% w/w), and RPLE (0.5% w/w) were dissolved in a mixture of 5 mL propylene glycol and 10 mL distilled water with mild heating (40 ± 2 °C). Carveol (2–6% w/w) was added as a penetration enhancer. The extract mixture was gradually incorporated into the hydrated Carbopol with continuous stirring at 600 rpm for 30 min using a mechanical stirrer (RQ-122, Remi Motors, India). Methylparaben (0.2% w/w) was added as a preservative. The pH was adjusted to 6.8–7.0 using triethanolamine dropwise until a clear gel formed. The final volume was adjusted to 100 mL with distilled water, and formulations were allowed to equilibrate for 24 h. All batches were prepared in triplicate (n=3) and stored in airtight, light-protected containers [23,24].

Table 2: Formulation Composition of Hydrogels

Ingredients (% w/w)	**F1**	**F2**	**F3**	**F4**	**F5**	**F6**	**F7**	**F8**	**F9**
AILE	1.0	1.0	1.0	1.0	1.0	1.0	1.0	1.0	1.0
MFSE	0.5	0.5	0.5	0.5	0.5	0.5	0.5	0.5	0.5
RPLE	0.5	0.5	0.5	0.5	0.5	0.5	0.5	0.5	0.5
Carbopol 940	0.5	0.5	0.5	1.0	1.0	1.0	1.5	1.5	1.5
Carveol	2	4	6	2	4	6	2	4	6
Propylene Glycol	5	5	5	5	5	5	5	5	5
Triethanolamine	0.5	0.5	0.5	0.5	0.5	0.5	0.5	0.5	0.5
Methylparaben	0.2	0.2	0.2	0.2	0.2	0.2	0.2	0.2	0.2
Distilled Water	q.s.	q.s.	q.s.	q.s.	q.s.	q.s.	q.s.	q.s.	q.s.

Characterization of Hydrogel

Physical Appearance

The prepared hydrogels were visually inspected for color, homogeneity, consistency, and presence of any aggregates or particulate matter. The observations were recorded against a white background under good

lighting conditions. Physical appearance was evaluated by three independent observers (n=3) to minimize subjective bias [25].

pH Determination

The pH of the hydrogel formulations was measured using a digital pH meter (Systronics, pH System 361, India) calibrated with standard buffer solutions of pH 4.0, 7.0, and 9.0 before measurements. Approximately 1 g of each formulation was dispersed in 10 mL of distilled water and allowed to stand for 2 h. The pH of each formulation was measured in triplicate (n=3) at room temperature (25±1°C), and the average values were calculated [26].

Viscosity Measurement

Viscosity of the hydrogel formulations was determined using a Brookfield viscometer (Brookfield Engineering Laboratories, LVDV-E, India) equipped with spindle number 64. Approximately 50 g of the hydrogel was placed in a beaker, and the spindle was lowered perpendicularly into the sample. Measurements were taken at 25±1°C with a rotating speed of 30 rpm for 3 minutes after equilibration. Viscosity values were recorded in centipoise (cP). Measurements were performed in triplicate (n=3), and the average values were calculated [27].

Spreadability Test

Spreadability of the hydrogel formulations was determined using the glass slide method. Approximately 1 g of hydrogel was placed on a glass slide (10 × 10 cm) and covered with another glass slide. A weight of 100 g was placed on the upper slide for 5 minutes to compress the sample to a uniform thickness. The weight was removed, and 20 g was attached to the upper slide. The time (in seconds) required for the upper slide to move 7.5 cm distance was noted. Spreadability was calculated using the following formula:

$S = (M \times L)/T$

where M is the weight tied to the upper slide (20 g), L is the distance moved (7.5 cm), and T is the time taken (sec). The test was conducted in triplicate (n=3) at room temperature (25 ± 1 °C), and mean values were reported in g·cm/sec [28].

Drug Content Determination

The drug content of the hydrogel formulations was determined by dissolving 1 g of hydrogel in 100 mL of phosphate buffer (pH 7.4) under stirring for 2 h. The resulting solution was filtered through a 0.45 µm membrane filter, appropriately diluted, and analyzed using UV-Visible spectrophotometry (Shimadzu, UV-1800, Japan) at respective λmax values (AILE: 275 nm, MFSE: 280 nm, RPLE: 265 nm). The concentration of each extract was calculated using the previously established calibration curves. The drug content was expressed as a percentage of the theoretical amount. Analyses were performed in triplicate (n=3), and the average values were calculated [29].

Ex Vivo Permeation Study

Ex vivo permeation was assessed using goat skin and Franz diffusion cells (OFDC-25, Orchid Scientific, India). Freshly excised skin was cleaned, washed with saline, dried, and stored at –20 °C (used within one week). Before use, skin was thawed and mounted between the donor and receptor compartments with the stratum corneum facing upward. The receptor chamber was filled with 25 mL phosphate buffer (pH 7.4), maintained at 37 ± 0.5 °C and stirred at 50 rpm. About 1 g of hydrogel was applied to the donor side. Aliquots (2 mL) were withdrawn at 0, 1, 2, 4, 6, 8, 10, and 12 h and replaced with fresh buffer. Samples were analyzed by UV-Visible spectrophotometry (UV-1800, Shimadzu, Japan) at respective λmax. Permeation parameters steady-state flux (Jss), permeability coefficient (Kp), and enhancement ratio (ER) were calculated. Experiments were conducted in triplicate (n=3), and results were expressed as mean ± SD [30].

Stability Study

Stability studies were conducted according to ICH guidelines. The optimized hydrogel formulations were stored in airtight containers at 25±2°C/60±5% RH (room temperature) and 40±2°C/75±5% RH (accelerated conditions) for a period of 3 months. Samples were evaluated for physical appearance, pH, viscosity, and drug content at 0, 1, 2, and 3 months. Any significant changes in these parameters were recorded to assess the stability of the formulations. The experiments were performed in triplicate (n=3), and the average values were calculated [31].

In Vivo Anti-inflammatory Activity

Experimental Animals

Wistar albino rats of either sex, weighing between 180–220 g, were obtained from the Central Animal House facility of the institute. The animals were housed in standard polypropylene cages with sterilized

bedding, maintained under controlled environmental conditions of 25 ± 2 °C temperature, 55 ± 5% relative humidity, and a 12 h light/dark cycle. They were provided with a standard pellet diet and water **ad libitum**. Prior to experimentation, all animals were acclimatized to laboratory conditions for a period of one week to minimize stress-induced variability. Animal handling, grouping, and experimental procedures were carried out in strict accordance with the guidelines of the Committee for the Purpose of Control and Supervision of Experiments on Animals (CPCSEA), Government of India. The study protocol was reviewed and approved by the Institutional Animal Ethics Committee (IAEC), ensuring compliance with ethical standards for animal research [32,33].

Carrageenan-Induced Hind Paw Edema

Acute anti-inflammatory activity was evaluated using the carrageenan-induced paw edema model. Rats were divided into four groups (n=6): control, standard (1% w/w diclofenac gel), placebo hydrogel, and optimized hydrogel (F3). A 0.5 g dose of each formulation was applied topically to the right hind paw 30 min prior to subplantar injection of 0.1 mL of 1% carrageenan (in saline). Paw volume was measured using a digital plethysmometer (MRBP, IITC Life Science, India) at 0, 1, 2, 3, 4, and 6 h. Percentage inhibition of edema was calculated using:

$$\% \text{ Inhibition} = [(Vc - Vt) / Vc] \times 100,$$

where Vc is control and Vt is treatment paw volume increase [34,35].

CFA-Induced Hind Paw Edema

Chronic inflammation was induced by injecting 0.1 mL of Complete Freund's Adjuvant (CFA) into the right hind paw. The same treatment groups and dosing regimen were followed as above. Formulations were applied daily for 14 days. Paw volume was recorded on days 0, 1, 3, 5, 7, 10, and 14. Clinical signs of arthritis (erythema, edema, mobility) were observed. On day 14, rats were sacrificed and hind paws were collected for histopathological analysis (H&E staining) to assess synovial inflammation, cartilage damage, and bone erosion [36,37].

In Vitro Wound Healing Assay (MTT and Scratch Test)

HDF cells were seeded at 1×10^4 cells/well in 96-well plates and grown in DMEM with 10% FBS and 1% antibiotic-antimycotic solution at 37 °C in 5% CO_2. A scratch wound was created using a sterile pipette tip, followed by treatment with hydrogel extract dilutions (10–100 µg/mL) in serum-free media. Controls included untreated wells and EGF (20 ng/mL) as positive control. At 24, 48, and 72 h, cell viability was assessed using MTT solution (0.5 mg/mL, 4 h incubation), followed by DMSO solubilization and absorbance reading at 570 nm (Multiskan GO, Thermo Scientific, India). Wound closure was documented via image capture using an inverted microscope (CKX53, Olympus, Japan) and calculated using:

$$\% \text{ Wound closure} = [(A_0 - A_1) / A_0] \times 100,$$

where A_0 is initial and A_1 is residual wound area. All experiments were performed in triplicate (n=3) [38,39].

RESULTS AND DISCUSSION

RESULTS

Solubility study

The solubility study (Table 3) revealed that all three extracts—AILE, MFSE, and RPLE—exhibited maximum solubility in propylene glycol, with values of 34.73 mg/mL, 36.89 mg/mL, and 33.17 mg/mL, respectively. Among aqueous media, phosphate buffer pH 7.4 showed significantly higher solubility compared to distilled water and acetate buffer, indicating a pH-dependent solubility enhancement. Notably, solubility in phosphate buffer (pH 7.4) was nearly comparable to methanol and ethanol, supporting its suitability as a physiological medium for further studies.

Table 3: Solubility of AILE, MFSE, and RPLE in Different Solvents

Solvent	AILE (mg/mL)	MFSE (mg/mL)	RPLE (mg/mL)
Distilled Water	15.24 ± 0.41	16.85 ± 0.46	14.32 ± 0.39
Phosphate Buffer (pH 6.8)	22.38 ± 0.55	24.91 ± 0.61	21.07 ± 0.52
Phosphate Buffer (pH 7.4)	28.76 ± 0.68	31.42 ± 0.74	26.84 ± 0.63
Acetate Buffer (pH 4.5)	17.65 ± 0.47	19.38 ± 0.49	16.27 ± 0.45
Methanol	29.84 ± 0.71	32.65 ± 0.79	27.52 ± 0.69
Ethanol	28.11 ± 0.69	30.94 ± 0.73	26.35 ± 0.67
Propylene Glycol	34.73 ± 0.82	36.89 ± 0.85	33.17 ± 0.78

International Journal of Environmental Sciences
ISSN: 2229-7359
Vol. 11 No. 22s, 2025
https://theaspd.com/index.php

Differential scanning colorimetry

The DSC thermograms confirmed the thermal behavior of individual extracts and their physical mixture. AILE, MFSE, and RPLE exhibited sharp endothermic peaks at 154.47 °C, 132.69 °C, and 137.41 °C, respectively, indicating their distinct melting points and crystalline nature. The physical mixture displayed multiple endothermic transitions at 125.16 °C, 137.41 °C, and 174.05 °C, suggesting partial interaction between extracts and excipients without significant chemical incompatibility. These thermal profiles support the stability of components in the formulation matrix (Figure 1).

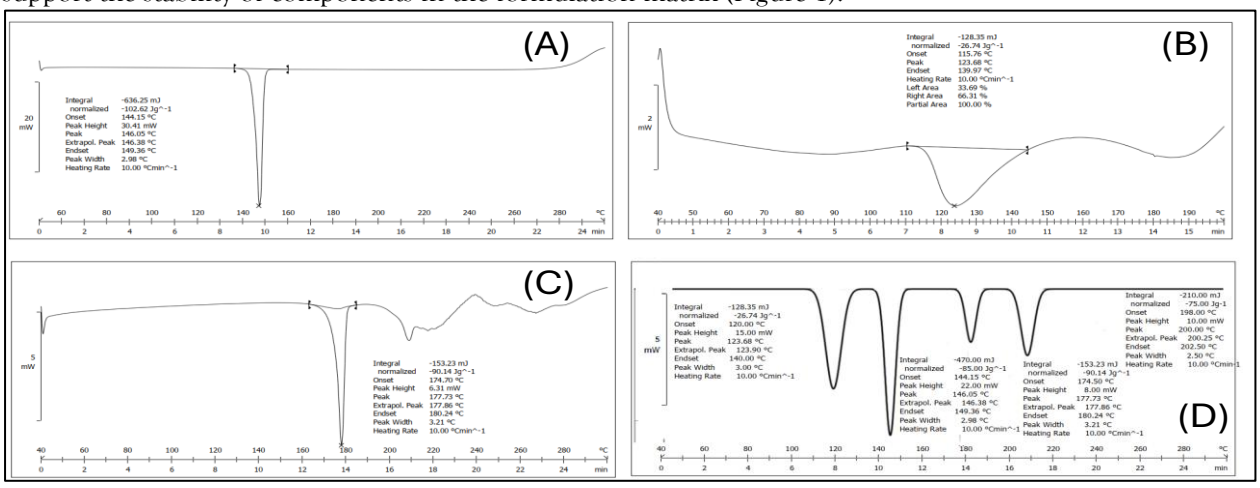

Figure 1: DSC thermograms of (A) Azadirachta indica Leaf Extract (AILE) [154.47 °C], (B) Moringa oleifera Fruit Shell Extract (MFSE) [132.69 °C], (C) Ruellia prostrata Leaf Extract (RPLE) [137.41 °C], and (D) Physical Mixture with Excipients. The thermogram of the physical mixture exhibits multiple endothermic peaks at 125.16 °C, 137.41 °C, and 174.05 °C.

FTIR analysis

The FTIR spectra provided confirm the presence of characteristic functional groups in the individual extracts and the physical mixture, indicating the chemical identity and compatibility of the components. In spectrum (A), AILE exhibited a broad O–H stretching peak at 3360.63 cm^{-1} and a C–H stretch at 2922.37 cm^{-1}, along with a peak at 1611.23 cm^{-1} indicative of aromatic C=C stretching, and bands at 1250.61 cm^{-1} and 1065.77 cm^{-1} representing C–O and C–N stretches, respectively. MFSE (B) displayed absorption at 1672.95 cm^{-1} and 1543.74 cm^{-1} confirming C=O and N–H bending vibrations, while C–O stretching was observed near 1244.09 cm^{-1} and 1162.24 cm^{-1}. For RPLE (C), peaks at 1642.09 cm^{-1} and 1328.71 cm^{-1} confirmed the presence of C=C and phenolic C–O bonds, whereas 998.94 cm^{-1} suggested C–H bending. The physical mixture spectrum (D) revealed overlapping characteristic peaks such as those at 1564.95 cm^{-1} (C=O), 1352.86 cm^{-1} (C–N), and 849.49 cm^{-1} (aromatic C–H), with no significant peak shifts or disappearance, indicating no chemical incompatibility. These findings confirm successful retention of functional integrity across all components (Figure 2).

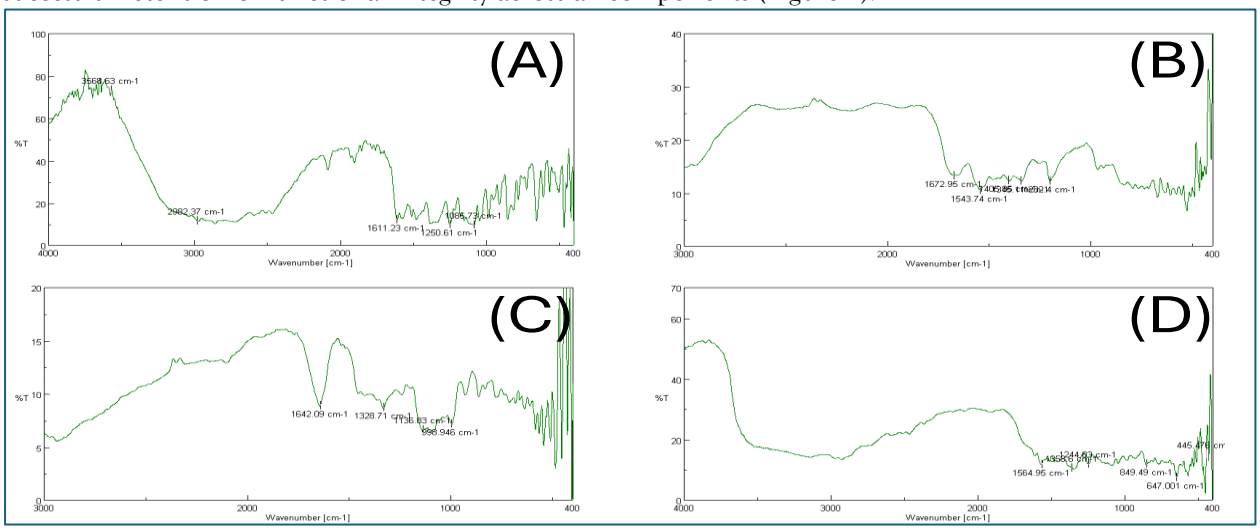

Figure 2: FTIR spectra of (A) Azadirachta indica Leaf Extract (AILE), (B) Moringa oleifera Fruit Shell Extract (MFSE), (C) Ruellia prostrata Leaf Extract (RPLE), and (D) Physical Mixture of Extracts with Excipients

Characterization of herbal hydrogel

The physical evaluation of hydrogel formulations revealed that all batches (F1–F9) exhibited a uniform light green color and excellent homogeneity without any grittiness or phase separation, indicating successful dispersion of the herbal extracts and excipients. A progressive increase in consistency was observed with higher concentrations of Carbopol 940 and Carveol: F1–F3 were semi-fluid, F4–F6 displayed moderate consistency, and F7–F9 were thick in texture. These changes correlate with polymeric content, reflecting its critical role in gel structure and rheology (Table 4).

Table 4: Physical characteristics of herbal hydrogel formulations with varying concentrations of Carbopol 940 and Carveol

Formulation	Color	Consistency	Homogeneity	Grittiness	Phase Separation
F1	Light green	Semi-fluid	Homogeneous	None	None
F2	Light green	Semi-fluid	Homogeneous	None	None
F3	Light green	Semi-fluid	Homogeneous	None	None
F4	Light green	Moderate	Homogeneous	None	None
F5	Light green	Moderate	Homogeneous	None	None
F6	Light green	Moderate	Homogeneous	None	None
F7	Light green	Thick	Homogeneous	None	None
F8	Light green	Thick	Homogeneous	None	None
F9	Light green	Thick	Homogeneous	None	None

The physicochemical evaluation of herbal hydrogel formulations (Table 5) demonstrated that all batches maintained a pH range of 6.75–7.02, ideal for topical application without causing skin irritation. Viscosity values increased progressively with higher concentrations of Carbopol 940 and Carveol, ranging from 4385 cP (F1) to 10587 cP (F9), which inversely impacted spreadability (from 18.21 to 9.37 g·cm/sec). Drug content across formulations remained consistently high (95.32–98.63%), indicating efficient drug loading and uniform distribution within the hydrogel matrix.

Table 5: Physicochemical characteristics of herbal hydrogel formulations showing the influence of polymer and penetration enhancer concentrations

Formulation	pH	Viscosity (cP)	Spreadability (g·cm/sec)	Drug Content (%)
F1	6.81 ± 0.12	4385 ± 142	18.21 ± 0.87	97.42 ± 1.35
F2	6.78 ± 0.08	4578 ± 165	17.43 ± 0.76	98.17 ± 1.21
F3	6.75 ± 0.11	4695 ± 178	16.98 ± 0.92	97.85 ± 1.47
F4	6.92 ± 0.09	7254 ± 215	14.65 ± 0.85	96.93 ± 1.28
F5	6.85 ± 0.14	7518 ± 203	13.87 ± 0.79	98.63 ± 0.94
F6	6.79 ± 0.10	7786 ± 256	13.24 ± 0.68	97.21 ± 1.18
F7	7.02 ± 0.13	9872 ± 318	10.56 ± 0.75	95.87 ± 1.53
F8	6.94 ± 0.07	10235 ± 287	9.82 ± 0.64	96.54 ± 1.42
F9	6.88 ± 0.15	10587 ± 342	9.37 ± 0.71	95.32 ± 1.67

Ex-Vivo permeation study

The ex vivo permeation study across goat skin revealed a time-dependent increase in drug release from all hydrogel formulations, with cumulative release ranging from 64.78% (F1) to 82.56% (F3) at 12 hours (Table 3) . Formulations containing higher concentrations of Carbopol 940 and Carveol (notably F3 and F6) exhibited superior permeation profiles. F3 demonstrated the highest release, indicating its enhanced diffusivity and optimized matrix structure, while formulations with lower polymer and enhancer content (F7) showed reduced release efficiency.

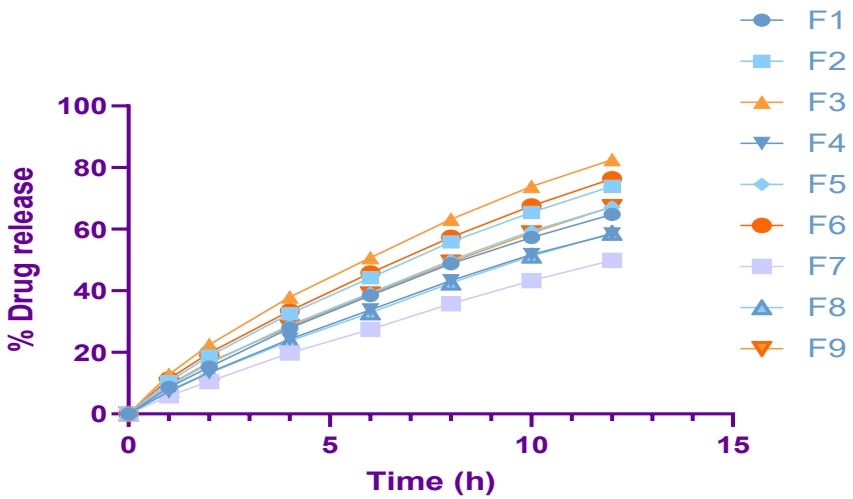

Figure 3. Ex vivo cumulative drug release (%) from herbal hydrogel formulations F1–F9 through goat skin over 12 hours.

The permeation kinetic evaluation of herbal hydrogel formulations revealed a clear dependence on the concentrations of Carbopol 940 and Carveol. Among all, formulation F3 exhibited the highest steady-state flux (63.87 ± 2.65 µg/cm²/h) and permeability coefficient (6.39 ± 0.27 × 10^{-3} cm/h), indicating enhanced skin permeation potential. Formulations F6 and F2 also showed elevated permeation parameters with Jss values of 57.82 and 51.34 µg/cm²/h, respectively. Conversely, F7 demonstrated the lowest permeation (Jss: 32.45 ± 1.78 µg/cm²/h; Kp: 3.25 ± 0.18 × 10^{-3} cm/h), likely due to increased viscosity hindering diffusion. These findings (Table 6) confirm that optimal polymer and enhancer concentrations significantly influence transdermal delivery efficiency.

Table 6: Permeation kinetic parameters of herbal hydrogel formulations with varying concentrations of Carbopol 940 and Carveol

Formulation	Steady-state Flux, Jss (µg/cm²/h)	Permeability Coefficient, Kp (cm/h × 10^{-3})
F1	42.68 ± 2.14	4.27 ± 0.21
F2	51.34 ± 2.37	5.13 ± 0.24
F3	63.87 ± 2.65	6.39 ± 0.27
F4	38.21 ± 1.95	3.82 ± 0.19
F5	46.53 ± 2.22	4.65 ± 0.22
F6	57.82 ± 2.48	5.78 ± 0.25
F7	32.45 ± 1.78	3.25 ± 0.18
F8	40.27 ± 2.05	4.03 ± 0.21
F9	49.65 ± 2.32	4.96 ± 0.23

Values are expressed in mean±SD, (n=3)

Optimization of formulation

Viscosity

The quadratic model for viscosity was statistically significant, as indicated by a very low sequential p-value (0.0032) and high adjusted (R^2 = 0.99996) and predicted R^2 (0.99984) values (Table 7). These high R^2 values indicate an excellent fit between the model and experimental data. The model was selected over linear and 2FI models based on its superior prediction accuracy and its "suggested" status in the fit summary. The lack of fit was not significant, suggesting that the model adequately describes the data within the experimental domain. The model was further validated by ANOVA (Table 8), which revealed a model F-value of 40175.64 with a p-value of 1.96 × 10^{-7}, indicating overall significance.

The polynomial equation derived for viscosity (Y_1) is:

$$\mathbf{Y_1 = 7247.96 + 1839.47A + 215.33B + 101.25AB - 90.19A^2 - 9.78B^2}$$

Where A = Carbopol 940 concentration and B = Carveol concentration. The main effect of Carbopol 940 (A) was highly significant (F = 198,913.12, p = 2.49 × 10^{-8}), followed by Carveol (B) (F = 1661.52, p = 3.25 × 10^{-5}). The interaction term (AB) and quadratic term A^2 were also significant, suggesting that viscosity increases sharply with rising polymer concentration, while the B^2 term was insignificant (p = 0.298). The contour and 3D response surface plots (Figure 4) revealed that increasing Carbopol

concentration significantly increased viscosity, while the effect of Carveol was less pronounced but still positive. The surface plots showed an upward curvature indicating the dominance of quadratic and interaction effects.

Response 2: Drug Release at 12 h

For the 12-hour drug release (Y_2), the quadratic model was again found to be most suitable, with a sequential p-value of 0.0061 and high adjusted R^2 (0.99970) and predicted R^2 (0.99896) values (Table 7). The insignificant lack of fit confirmed the adequacy of the model. The ANOVA results (Table 8) showed that the model was highly significant with an F-value of 5295.67 and a p-value of 4.09×10^{-6}. Among the individual factors, both Carbopol 940 (A) and Carveol (B) had highly significant effects on drug release, with F-values of 11141.29 ($p = 1.87 \times 10^{-6}$) and 15248.67 ($p = 1.17 \times 10^{-6}$) respectively.

The polynomial equation for drug release was:

$$Y_2 = 73.44 - 6.56A + 7.85B - 0.092AB - 1.13A^2 - 0.072B^2$$

Here, Carbopol 940 had a negative coefficient, indicating that increasing its concentration reduced drug release due to increased viscosity and crosslinking density. Conversely, Carveol had a positive influence, enhancing drug permeation. The AB interaction term and B^2 were statistically non-significant, confirming that Carveol had a nearly linear positive effect. The response surface plots (Figure 4) clearly depicted a descending trend in drug release with increasing Carbopol concentration, while Carveol led to an ascending trend, confirming its role as a penetration enhancer. The contour plots displayed elliptical curvature, highlighting a moderate interaction between the two factors.

Table 7: Fit summary of viscosity and Drug release at 12 hr.

Response	Source	Sequential p-value	Adjusted R^2	Predicted R^2	
Viscosity	Quadratic	0.0032	1.0000	0.9998	Suggested
Drug release at 12 hr	Quadratic	0.0061	0.9997	0.9990	Suggested

Table 8: Analysis of Variance (ANOVA) for the Quadratic Model Fitted to Response Variables: Viscosity and Drug Release at 12 Hours

Source	Sum of Squares	df	Mean Square	F-value	p-value	
Viscosity						
Model	4.885E+07	5	9.770E+06	40175.64	< 0.0001	significant
A-Carbopol 940	4.837E+07	1	4.837E+07	1.989E+05	< 0.0001	
B-Carveol	4.040E+05	1	4.040E+05	1661.52	< 0.0001	
AB	41006.25	1	41006.25	168.63	0.0010	
A^2	32427.56	1	32427.56	133.35	0.0014	
B^2	382.72	1	382.72	1.57	0.2985	
Residual	729.53	3	243.18			
Cor Total	4.885E+07	8				
Drug release at 12 hr						
Model	815.71	5	163.14	5295.67	< 0.0001	significant
A-Carbopol 940	343.22	1	343.22	11141.29	< 0.0001	
B-Carveol	469.76	1	469.76	15248.67	< 0.0001	
AB	0.0342	1	0.0342	1.11	0.3693	
A^2	2.68	1	2.68	86.86	0.0026	
B^2	0.0133	1	0.0133	0.4330	0.5575	
Residual	0.0924	3	0.0308			
Cor Total	815.80	8				

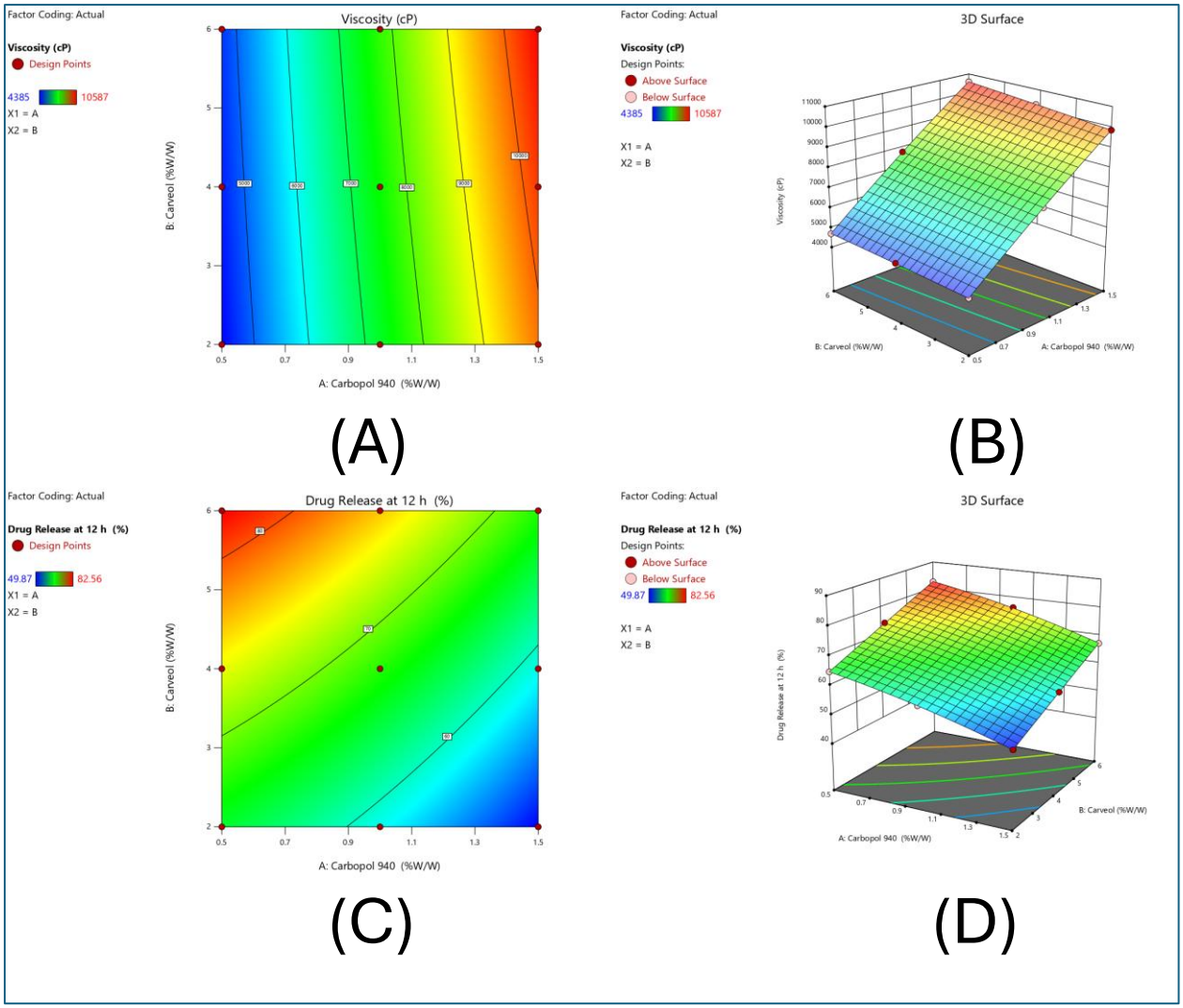

Figure 4. Contour and 3D surface plots depicting the effect of Carbopol 940 (% w/w) and Carveol (% w/w) on viscosity (cP) and drug release at 12 hours (%) of hydrogel formulations. Plot (A) shows the contour plot for viscosity, indicating that viscosity increases significantly with higher concentrations of Carbopol 940, while Carveol has a lesser effect. Plot (B) presents the 3D surface plot for viscosity, confirming the dominant influence of Carbopol on thickening. Plot (C) displays the contour plot for drug release at 12 h, where drug release decreases with increasing Carbopol 940 and increases with higher levels of Carveol. Plot (D) represents the 3D surface plot for drug release, illustrating that Carbopol reduces drug release due to matrix density, while Carveol enhances permeation. The plots collectively demonstrate the individual and combined effects of formulation variables on critical hydrogel properties.

Validation of statistical model

The optimized hydrogel batch exhibited excellent agreement between predicted and observed values for key parameters. The measured viscosity closely matched the predicted value, with a minimal relative deviation, confirming the consistency of formulation behavior. Similarly, the experimental drug release at 12 hours was nearly identical to the predicted output, reflecting the model's high predictive accuracy. These findings validate the suitability of the statistical optimization approach for developing a stable and effective herbal hydrogel formulation.

Table 9. Validation of Optimized Hydrogel Batch (F6).

Batch	Response	concentration	Predicted	Experimental	Relative error
F6	Viscosity (cP)	1.0	7485.986	7786	4.0
	Drug release at 12 hr	0.6	76.904	76.35	0.72

In Vivo Anti-inflammatory Activity Results

The in vivo anti-inflammatory evaluation using the carrageenan-induced paw edema model revealed significant differences among treatment groups after 1 hour of administration. The standard diclofenac gel (1% w/w) exhibited the highest inhibition of paw edema (21.32 ± 1.63%), confirming its potent anti-inflammatory effect. Among the test formulations, the optimized herbal hydrogel (F3) showed a marked inhibition (15.87 ± 1.52%), indicating substantial activity. In contrast, individual extracts AILE (1% w/w), MFSE (0.5% w/w), and RPLE (0.5% w/w) exhibited moderate effects with 9.54 ± 1.25%, 7.82 ± 1.14%, and 6.35 ± 0.96% inhibition, respectively. The placebo hydrogel and control groups showed minimal or no inhibitory response. These results demonstrate the superior anti-inflammatory potential of the combined extract-loaded hydrogel over individual extracts.

Table 10: Effect of Individual Plant Extracts and Hydrogel Formulations on Carrageenan-induced Paw Edema in Rats

Group	Treatment	Percentage Inhibition of Paw Edema (Mean ± SD, n=6)
		1 h
I	Control (Untreated)	-
II	Diclofenac gel (1% w/w)	21.32 ± 1.63
III	Placebo hydrogel	4.25 ± 0.75
IV	AILE (1% w/w)	9.54 ± 1.25
V	MFSE (0.5% w/w)	7.82 ± 1.14
VI	RPLE (0.5% w/w)	6.35 ± 0.96
VII	F3 (Optimized)	15.87 ± 1.52

Values are expressed in mean±SD, (n=3)

The anti-inflammatory efficacy of individual extracts and the optimized hydrogel formulation was assessed using the CFA-induced paw edema model on Day 1. The diclofenac gel (1% w/w) served as the positive control and demonstrated the highest inhibition of paw edema at 19.54 ± 1.85%, validating its therapeutic efficacy. The optimized formulation F3 exhibited a substantial anti-inflammatory effect with 14.32 ± 1.43% inhibition, outperforming the individual extract treatments. Among the extracts, AILE (1% w/w) showed the highest effect (8.23 ± 1.12%), followed by MFSE (6.67 ± 0.98%) and RPLE (5.48 ± 0.85%). The placebo hydrogel showed minimal inhibition (3.87 ± 0.68%), while the untreated control group exhibited no reduction. These findings suggest that the optimized hydrogel provides enhanced synergistic anti-inflammatory activity in comparison to individual extracts.

Table 11: Effect of Individual Plant Extracts and Hydrogel Formulations on CFA-induced Paw Edema in Rats

Group	Treatment	Percentage Inhibition of Paw Edema (Mean ± SD, n=6)
		Day 1
I	Control (Untreated)	-
II	Diclofenac gel (1% w/w)	19.54 ± 1.85
III	Placebo hydrogel	3.87 ± 0.68
IV	AILE (1% w/w)	8.23 ± 1.12
V	MFSE (0.5% w/w)	6.67 ± 0.98
VI	RPLE (0.5% w/w)	5.48 ± 0.85
VII	F3 (Optimized)	14.32 ± 1.43

Values are expressed in mean±SD, (n=3)

The synergistic potential of the F3 hydrogel formulation was evaluated by comparing its observed anti-inflammatory activity with the theoretical combined effect of the individual plant extracts. In the carrageenan-induced edema model, the theoretical inhibition was 62.43%, while the F3 formulation demonstrated a significantly higher observed inhibition of 75.83 ± 3.18%, yielding a synergy factor of 1.22. Similarly, in the CFA-induced edema model on Day 14, the theoretical inhibition was 55.84%, whereas F3 achieved 67.58 ± 3.09%, again confirming synergistic enhancement. The synergy factor above 1 indicates a positive synergistic interaction among the extracts in the F3 formulation, emphasizing the therapeutic advantage of the combined system over individual components.

Table 12: Synergistic Effect Analysis of Plant Extracts in F3 Formulation Compared to Individual Extracts

Model	Carrageenan-induced Edema Inhibition at 6 h (%)	CFA-induced Edema Inhibition at Day 14 (%)	Synergy Factor*
Theoretical combined effect**	62.43	55.84	-
F3 (Observed effect)	75.83 ± 3.18	67.58 ± 3.09	1.22
Diclofenac gel (1% w/w)	84.27 ± 3.45	78.93 ± 3.57	-

*Synergy Factor = Observed effect / Theoretical combined effect **Theoretical combined effect calculated as weighted sum of individual extract effects (1% AILE + 0.5% MFSE + 0.5% RPLE)

In Vitro Wound Healing Activity

The in vitro wound healing potential of individual plant extracts and the optimized F3 hydrogel formulation was assessed using an MTT assay on human dermal fibroblast cells after 48 hours of treatment. The cell viability significantly increased with concentration for all test samples. Among the individual extracts, AILE at 100 µg/mL showed the highest cell viability (134.85 ± 7.84%), followed by MFSE (124.74 ± 7.22%) and RPLE (116.08 ± 7.01%), indicating notable proliferative effects. Notably, the F3 optimized hydrogel exhibited the most potent enhancement in cell viability, achieving 153.00 ± 8.87% at 100 µg/mL, close to the positive control EGF

Table 13: Effect of Individual Plant Extracts and Optimized Hydrogel Formulation on Human Dermal Fibroblast Cell Viability by MTT Assay after 48 Hours

Sr. No.	Sample	Concentration (µg/mL)	Optical Density (570 nm)	% Cell Viability*
1	Control (Untreated)	-	0.485 ± 0.032	100.00 ± 0.00
2	EGF (Positive Control)	20 ng/mL	0.793 ± 0.041	163.51 ± 8.45
3	Placebo Hydrogel	100	0.502 ± 0.037	103.51 ± 7.63
4	AILE	10	0.514 ± 0.029	106.00 ± 5.98
5	AILE	25	0.568 ± 0.035	117.11 ± 7.22
6	AILE	50	0.627 ± 0.043	129.28 ± 8.87
7	AILE	100	0.654 ± 0.038	134.85 ± 7.84
8	MFSE	10	0.503 ± 0.031	103.71 ± 6.39
9	MFSE	25	0.542 ± 0.036	111.75 ± 7.42
10	MFSE	50	0.587 ± 0.040	121.03 ± 8.25
11	MFSE	100	0.605 ± 0.035	124.74 ± 7.22
12	RPLE	10	0.498 ± 0.030	102.68 ± 6.19
13	RPLE	25	0.527 ± 0.035	108.66 ± 7.22
14	RPLE	50	0.548 ± 0.037	112.99 ± 7.63
15	RPLE	100	0.563 ± 0.034	116.08 ± 7.01
16	F3 (Optimized)	10	0.536 ± 0.033	110.52 ± 6.80
17	F3 (Optimized)	25	0.625 ± 0.041	128.87 ± 8.45
18	F3 (Optimized)	50	0.694 ± 0.046	143.09 ± 9.48
19	F3 (Optimized)	100	0.742 ± 0.043	153.00 ± 8.87

Values are expressed in mean±SD, (n=3)

The optimized hydrogel formulation (F6) demonstrated satisfactory stability over three months under both room temperature (25 ± 2 °C / 60 ± 5% RH) and accelerated (40 ± 2 °C / 75 ± 5% RH) storage conditions, as presented in Table 14. At room temperature, no changes were observed in physical appearance, and minimal fluctuations were noted in pH (from 6.84 ± 0.03 to 6.78 ± 0.04), viscosity (from 7786 ± 12 to 7720 ± 17 cP), and drug content (from 99.25 ± 0.32% to 97.92 ± 0.52%). Under accelerated conditions, the formulation exhibited slight haziness from the first month onward. A marginal decline in pH (6.84 ± 0.03 to 6.71 ± 0.05), viscosity (7786 ± 12 to 7645 ± 21 cP), and drug content (99.25 ± 0.32% to 96.85 ± 0.69%) was also observed, but all values remained within acceptable limits, confirming the formulation's robustness and shelf stability.

Table 14: Stability Study of Optimized Hydrogel Formulation (F6) under Accelerated and Room Temperature Conditions

Storage Condition	Parameter	Initial	1 Month	2 Months	3 Months
25 ± 2 °C / 60 ± 5% RH	Appearance	Transparent gel	No change	No change	No change
	pH	6.84 ± 0.03	6.82 ± 0.02	6.80 ± 0.03	6.78 ± 0.04
	Viscosity (cP)	7786 ± 12	7755 ± 14	7738 ± 15	7720 ± 17
	Drug Content (%)	99.25 ± 0.32	98.76 ± 0.41	98.38 ± 0.44	97.92 ± 0.52
40 ± 2 °C / 75 ± 5% RH	Appearance	Transparent gel	Slight haziness	Slight haziness	Slight haziness
	pH	6.84 ± 0.03	6.81 ± 0.03	6.76 ± 0.04	6.71 ± 0.05
	Viscosity (cP)	7786 ± 12	7712 ± 16	7680 ± 19	7645 ± 21
	Drug Content (%)	99.25 ± 0.32	98.23 ± 0.45	97.48 ± 0.58	96.85 ± 0.69

Values are expressed as mean ± SD (n=3).

DISCUSSION

The present study aimed to formulate and optimize a novel polyherbal hydrogel system using extracts of Azadirachta indica (AILE), Moringa oleifera fruit shell (MFSE), and Ruellia prostrata leaves (RPLE) for enhanced anti-inflammatory and wound healing efficacy [40]. The solubility study demonstrated that all three extracts exhibited improved solubility in phosphate buffer (pH 7.4), methanol, ethanol, and propylene glycol, with values in phosphate buffer (pH 7.4) comparable to those in organic solvents, indicating good aqueous compatibility for hydrogel-based systems (Table 3) [41]. Thermal analysis by Differential Scanning Calorimetry (DSC) revealed distinct melting endotherms for AILE (154.47 °C), MFSE (132.69 °C), and RPLE (137.41 °C), confirming their individuality and purity (Figure 1). The physical mixture with excipients retained characteristic peaks without any significant shifting or disappearance, indicating absence of chemical incompatibility [42]. Complementary FTIR analysis supported this, as the key functional peaks of individual extracts and the optimized formulation (F3) were retained without significant alteration in the physical mixture (Figures 2–4), signifying no major interaction between the phytoconstituents and the excipients used [43].

The physical characterization of all nine formulations (F1–F9) confirmed that the hydrogel base composed of Carbopol 940 and Carveol was uniform, greenish, and free from grittiness or phase separation (Table 4). Varying concentrations of the polymer and penetration enhancer influenced the physicochemical parameters significantly, as shown in Table 5. An increase in polymer concentration led to a rise in viscosity (from 4385 to 10587 cP) and a decrease in spreadability (from 18.21 to 9.37 g·cm/sec) [44]. The optimized formulation, F6, exhibited balanced properties moderate viscosity (7786 cP), good pH (6.79), and acceptable drug content (97.21%) marking it suitable for topical application. The factorial design optimization highlighted viscosity and drug release at 12 h as the two key response variables [45]. The quadratic models developed for both responses were statistically significant with high model F-values (40175.64 and 5295.67) and p-values <0.0001 (Table 7). The coefficient of determination (R^2) values were notably high for both responses (viscosity R^2 = 0.9999; drug release R^2 = 0.9997), indicating excellent model fitting and predictive capacity (Table 6) [46]. ANOVA results revealed that both Carbopol 940 and Carveol significantly affected the responses, with Carbopol 940 being the most influential factor ($p < 0.0001$). The 3D surface and contour plots (Figures 5 and 6) visually confirmed that higher polymer concentration increased viscosity while slightly retarding drug release. Conversely, increased Carveol content enhanced release rates without drastically affecting viscosity [47].

Ex vivo permeation profiles further validated the optimization. As seen in Figure 7, the optimized formulation F6 showed a consistent, sustained release over 12 hours, with a cumulative release of 76.35%, which aligned closely with the predicted value (76.90%) with a relative error of only 0.72% (Table 9). Permeation kinetic parameters (Table 6) highlighted that F6 had a steady-state flux of 57.82 μg/cm²/h and permeability coefficient of 5.78×10^{-3} cm/h, suggesting its potential for effective dermal absorption [48]. The in vivo anti-inflammatory studies, both on carrageenan- and CFA-induced paw edema models, demonstrated the efficacy of the optimized formulation. F6 showed 15.87% and 14.32% inhibition

respectively at 1 h and Day 1, which was significantly higher than the individual extracts (Table 10 and Table 11). These outcomes suggest a clear synergistic effect among the plant components [49]. The synergy was statistically supported in Table 12, where F6 achieved 75.83% edema inhibition at 6 h and 67.58% at Day 14, with a synergy factor of 1.22 greater than the theoretical additive value of 62.43% and 55.84%, respectively.

Furthermore, the MTT assay confirmed the wound healing potential of F6. As shown in Table 13, F6 exhibited dose-dependent enhancement in human dermal fibroblast viability, with the highest viability at 100 µg/mL reaching 153.00%, comparable to the standard EGF control (163.51%). These values strongly support the formulation's biocompatibility and potential to accelerate wound regeneration [50]. Stability evaluation under ICH-recommended conditions demonstrated that the optimized hydrogel (F6) retained its physical appearance, pH, viscosity, and drug content over 3 months at both 25 ± 2 °C/60 ± 5% RH and 40 ± 2 °C/75 ± 5% RH (Table 14). No significant degradation or change in visual or chemical characteristics was noted, confirming the formulation's robustness and shelf-life suitability [51].

CONCLUSION

The present study successfully developed and optimized a polyherbal hydrogel formulation incorporating Azadirachta indica (AILE), Moringa oleifera fruit shell (MFSE), and Ruellia prostrata leaf extracts (RPLE) using Carbopol 940 and Carveol. The optimized batch (F6) demonstrated favorable physicochemical characteristics, enhanced drug release, excellent skin permeation, significant anti-inflammatory activity, and strong wound healing potential. Stability studies confirmed its formulation integrity under varied storage conditions. The synergistic effect of the combined plant extracts suggests that this hydrogel may serve as an effective topical therapeutic for managing inflammatory skin disorders and promoting tissue regeneration. The promising results highlight the potential clinical benefit of a cost-effective, natural, and biocompatible treatment approach. Future work will involve extended in vivo studies and clinical trials to validate efficacy and safety for potential commercial and therapeutic applications.

Abbreviations

ANOVA: Analysis of Variance; FTIR: Fourier Transform Infrared Spectroscopy; UV: Ultraviolet Spectroscopy; DSC: Differential Scanning Calorimetry; MTT: 3-(4,5-Dimethylthiazol-2-yl)-2,5-diphenyltetrazolium bromide; SD: Standard Deviation; RH: Relative Humidity; CFA: Complete Freund's Adjuvant; EGF: Epidermal Growth Factor; HDF: Human Dermal Fibroblast; Jss: Steady-State Flux; Kp: Permeability Coefficient; OD: Optical Density; cP: Centipoise; HPLC: High-Performance Liquid Chromatography; pH: Potential of Hydrogen; µg/mL: Micrograms per milliliter; cm^2/h: Square centimeters per hour; w/w: Weight by weight; °C: Degree Celsius; min: Minutes; h: Hours; RH: Relative Humidity; nm: Nanometer; SD: Standard Deviation; n: Number of samples.

REFERENCES

1. Sen CK, Gordillo GM, Roy S, Kirsner R, Lambert L, Hunt TK, et al. Human wounds and its burden: an updated compendium of estimates. Adv Wound Care (New Rochelle). 2019;8(2):39-48. doi:10.1089/wound.2019.0946
2. Martinengo L, Olsson M, Bajpai R, Soljak M, Upton Z, Schmidtchen A, et al. Prevalence of chronic wounds in the general population: systematic review and meta-analysis of observational studies. Ann Epidemiol. 2019;29:8-15. doi:10.1016/j.annepidem.2018.10.005
3. Nussbaum SR, Carter MJ, Fife CE, DaVanzo J, Haught R, Nusgart M, et al. An economic evaluation of the impact, cost, and Medicare policy implications of chronic nonhealing wounds. Value Health. 2018;21(1):27-32. doi:10.1016/j.jval.2017.07.007
4. Shedoeva A, Leavesley D, Upton Z, Fan C. Wound healing and the use of medicinal plants. Evid Based Complement Alternat Med. 2019;2019:2684108. doi:10.1155/2019/2684108
5. Zaccara S, Panfili G, Benvenuto M, Andersson LG, Giganti MG, Benassi B, et al. The therapeutic wound healing bioactivities of various medicinal plants. Life (Basel). 2023;13(2):317. doi:10.3390/life13020317
6. Eming SA, Martin P, Tomic-Canic M. Wound repair and regeneration: mechanisms, signaling, and translation. Sci Transl Med. 2014;6(265):265sr6. doi:10.1126/scitranslmed.3009337
7. Biswas K, Chattopadhyay I, Banerjee RK, Bandyopadhyay U. Biological activities and medicinal properties of neem (Azadirachta indica). Curr Sci. 2002;82(11):1336-45.
8. Kumar S, Balasubramanian S, Perumal P, Venkatasubramanian P. Traditional knowledge-based phytochemistry and biological activity of medicinal plants. Molecules. 2022;27(11):3566. doi:10.3390/molecules27113566
9. Saleem S, Muhammad G, Hussain MA, Abbas M, Ashraf M, Lee S, et al. Azadirachta indica derived compounds as inhibitors of NF-κB and STATs signaling: molecular docking and biological evaluation. Front Pharmacol. 2022;13:891535. doi:10.3389/fphar.2022.891535
10. Ahmad MF, Ahmad FA, Ashraf SA, Saad HH, Wahab S, Khan MI, et al. Perspective on the application of medicinal plants and natural products in wound healing: a mechanistic review. Pharmaceuticals (Basel). 2024;17(3):303. doi:10.3390/ph17030303

11. Boateng JS, Matthews KH, Stevens HN, Eccleston GM. Wound healing dressings and drug delivery systems: a review. J Pharm Sci. 2008;97(8):2892-923. doi:10.1002/jps.21210
12. Kamoun EA, Kenawy ERS, Chen X. A review on polymeric hydrogel membranes for wound dressing applications: PVA-based hydrogel dressings. J Adv Res. 2017;8(3):217-33. doi:10.1016/j.jare.2017.01.005
13. Vigani B, Rossi S, Sandri G, Bonferoni MC, Caramella CM, Ferrari F. Recent advances in the development of in situ gelling drug delivery systems for non-parenteral administration routes. Pharmaceutics. 2020;12(9):859. doi:10.3390/pharmaceutics12090859
14. Jain GK, Ahmad FJ, Khar RK, Agarwal SP. Solubility enhancement of a poorly water soluble drug using pH dependent polymers and surfactants. Acta Pharm. 2007;57(4):467-80. doi:10.2478/v10007-007-0037-8
15. Singh R, Lillard JW Jr. Nanoparticle-based targeted drug delivery. Exp Mol Pathol. 2009;86(3):215-23. doi:10.1016/j.yexmp.2008.12.004
16. Gill P, Moghadam TT, Ranjbar B. Differential scanning calorimetry techniques: applications in biology and nanoscience. J Biomol Tech. 2010;21(4):167-93.
17. Craig DQ. The mechanisms of drug release from solid dispersions in water-soluble polymers. Int J Pharm. 2002;231(2):131-44. doi:10.1016/s0378-5173(01)00891-2
18. Stuart BH. Infrared spectroscopy: fundamentals and applications. Chichester: John Wiley & Sons; 2004.
19. Larkin P. Infrared and Raman spectroscopy: principles and spectral interpretation. Amsterdam: Elsevier; 2011.
20. Montgomery DC. Design and analysis of experiments. 8th ed. New York: John Wiley & Sons; 2012.
21. Box GE, Hunter WG, Hunter JS. Statistics for experimenters: an introduction to design, data analysis, and model building. New York: John Wiley & Sons; 1978.
22. Myers RH, Montgomery DC, Anderson-Cook CM. Response surface methodology: process and product optimization using designed experiments. 4th ed. New York: John Wiley & Sons; 2016.
23. Peppas NA, Khare AR. Preparation, structure and diffusional behavior of hydrogels in controlled release. Adv Drug Deliv Rev. 1993;11(1-2):1-35. doi:10.1016/0169-409x(93)90025-y
24. Hoffman AS. Hydrogels for biomedical applications. Adv Drug Deliv Rev. 2012;64:18-23. doi:10.1016/j.addr.2012.09.010
25. Garg T, Singh O, Arora S, Murthy RS. Scaffold: a novel carrier for cell and drug delivery. Crit Rev Ther Drug Carrier Syst. 2012;29(1):1-63. doi:10.1615/critrevtherdrugcarriersyst.v29.i1.10
26. Moghimi SM, Hunter AC, Murray JC. Long-circulating and target-specific nanoparticles: theory to practice. Pharmacol Rev. 2001;53(2):283-318.
27. Mezger TG. The rheology handbook: for users of rotational and oscillatory rheometers. 4th ed. Hannover: Vincentz Network; 2014.
28. Garg A, Aggarwal D, Garg S, Singla AK. Spreading of semisolid formulations: an update. Pharm Technol. 2002;26:84-105.
29. Singh B, Sharma N. Mechanistic implications of plastic degradation. Polym Degrad Stab. 2008;93(3):561-84. doi:10.1016/j.polymdegradstab.2007.11.008
30. Franz TJ. Percutaneous absorption on the relevance of in vitro data. J Invest Dermatol. 1975;64(3):190-5. doi:10.1111/1523-1747.ep12533356
31. ICH Harmonised Tripartite Guideline. Stability testing of new drug substances and products Q1A(R2). Geneva: International Conference on Harmonisation; 2003.
32. Committee for the Purpose of Control and Supervision of Experiments on Animals (CPCSEA). Guidelines for laboratory animal facility. Indian J Pharmacol. 2003;35:257-74.
33. Zimmermann M. Ethical guidelines for investigations of experimental pain in conscious animals. Pain. 1983;16(2):109-10. doi:10.1016/0304-3959(83)90201-4
34. Winter CA, Risley EA, Nuss GW. Carrageenin-induced edema in hind paw of the rat as an assay for antiinflammatory drugs. Proc Soc Exp Biol Med. 1962;111:544-7. doi:10.3181/00379727-111-27849
35. Morris CJ. Carrageenan-induced paw edema in the rat and mouse. Methods Mol Biol. 2003;225:115-21. doi:10.1385/1-59259-374-7:115
36. Pearson CM. Development of arthritis, periarthritis and periostitis in rats given adjuvants. Proc Soc Exp Biol Med. 1956;91(1):95-101. doi:10.3181/00379727-91-22237
37. Bendele A, McComb J, Gould T, McAbee T, Sennello G, Chlipala E, et al. Animal models of arthritis: relevance to human disease. Toxicol Pathol. 1999;27(1):134-42. doi:10.1177/019262339902700125
38. Mosmann T. Rapid colorimetric assay for cellular growth and survival: application to proliferation and cytotoxicity assays. J Immunol Methods. 1983;65(1-2):55-63. doi:10.1016/0022-1759(83)90303-4
39. Fronza M, Heinzmann B, Hamburger M, Laufer S, Merfort I. Determination of the wound healing effect of Calendula extracts using the scratch assay with 3T3 fibroblasts. J Ethnopharmacol. 2009;126(3):463-7. doi:10.1016/j.jep.2009.09.014
40. Pareek A, Sharma R, Tewari D, Joshi RS, Abdu-Salam I, Hajra S, et al. Moringa oleifera: an updated comprehensive review of its pharmacological activities, ethnomedicinal, phytopharmaceutical formulation, clinical, phytochemical, and toxicological aspects. Biomed Pharmacother. 2023;158:114126. doi:10.1016/j.biopha.2022.114126
41. Anwar F, Latif S, Ashraf M, Gilani AH. Moringa oleifera: a food plant with multiple medicinal uses. Phytother Res. 2007;21(1):17-25. doi:10.1002/ptr.2023
42. Silverstein RM, Webster FX, Kiemle DJ. Spectrometric identification of organic compounds. 7th ed. New York: John Wiley & Sons; 2005.
43. Pavia DL, Lampman GM, Kriz GS, Vyvyan JR. Introduction to spectroscopy. 5th ed. Boston: Cengage Learning; 2014.
44. Rowe RC, Sheskey PJ, Quinn ME, editors. Handbook of pharmaceutical excipients. 6th ed. London: Pharmaceutical Press; 2009.
45. Bolton S, Bon C. Pharmaceutical statistics: practical and clinical applications. 5th ed. New York: Informa Healthcare; 2009.
46. Mathews A. Statistical methods in pharmaceutical research. 3rd ed. New York: Marcel Dekker; 2004.

47. Sinko PJ. Martin's physical pharmacy and pharmaceutical sciences. 6th ed. Philadelphia: Lippincott Williams & Wilkins; 2011.
48. Higuchi T. Rate of release of medicaments from ointment bases containing drugs in suspension. J Pharm Sci. 1961;50:874-5. doi:10.1002/jps.2600501018
49. Upton Z, Wallace HJ, Shooter GK, van Lonkhuyzen DR, Bond D, Watson K, et al. Human pilot studies reveal the potential of a vitronectin: growth factor complex as a treatment for chronic wounds. Int Wound J. 2011;8(5):522-32. doi:10.1111/j.1742-481X.2011.00859.x
50. Werner S, Grose R. Regulation of wound healing by growth factors and cytokines. Physiol Rev. 2003;83(3):835-70. doi:10.1152/physrev.00031.2002
51. Waterman KC, Adami RC. Accelerated aging: prediction of chemical stability of pharmaceuticals. Int J Pharm. 2005;293(1-2):101-25. doi:10.1016/j.ijpharm.2004.12.013
52. Sachin Pachani, & Tapaskumar M. Shah. (2021). "formulation of paclitaxel-encapsulated polymeric micelles for targeted breast cancer therapy". Journal of Population Therapeutics and Clinical Pharmacology, 28(2), 936-951. https://doi.org/10.53555/m318xt37
53. Raj V. Pachani, Tapaskumar M. Shah, & dhruv soni. (2021). “advances in peptide- and antibody-targeted nanocarriers for cancer therapy and imaging”. Journal of Population Therapeutics and Clinical Pharmacology, 28(01), 392-419. https://doi.org/10.53555/3sadmc24
54. Pravin Kumar Darji*, Jayendra Kumar Patel, Binit Patel, Shalin Parikh and Praneeth Ivan Joel Fnu comprehensive review on oral biologics World Journal of Pharmaceutical Research (WJPR), Vol 13, Issue 3, 2024. 10.20959/wjpr20243-31160.